Design and Control of a Fault Tolerant Permanent Magnet Motor with Independently Optimized Phase and Pole Counts

Shima Hasanpour, Shrikesh Sheshaprasad, Matthew C. Gardner, Matthew Johnson, Bryton Praslicka, and Hamid A. Toliyat

Abstract – **Multi-phase motors offer a high reliability solution for safety-critical applications as they can operate under some fault conditions with reduced performance. Permanent magnet synchronous motors (PMSMs) provide high torque density and efficiency. This study performed a thorough parametric analysis using 2-D magnetostatic and transient finite element analysis (FEA) to individually optimize PMSMs with double-layer or single-layer windings. There is no defined relation between rotor pole pair and stator phase numbers for better optimization. This paper uses an H-bridge for each phase to control the phases independently and introduces an optimal approach for power compensation during the open circuit fault. This method achieves the minimum torque ripple and the minimum increase in DC copper losses. As expected, the topology using a double-layer winding and a Halbach array was found to outperform the other topologies with regards to torque density and efficiency.**

Index Terms— **AC motors, Brushless motors, Electric motors, Fault diagnosis, Finite element analysis, Optimization, Permanent magnet motors, Reliability, Traction motors.**

I. Introduction

Multi-phase motors are a common solution for applications requiring high reliability, such as aerospace, traction, and military vehicles [1]-[8]. Increasing the number of phases in a motor allows the motor to continue operating with less of a performance penalty when a fault occurs. Multi-phase permanent magnet synchronous motors (PMSMs), such as those shown in Fig. 1, are advantageous for these applications due to their high power density and efficiency. Most existing literature analyzes the performance of a few designs that are not necessarily optimized for specific rotor pole pair counts or stator phase numbers. Many previous studies [7]-[17] investigate multi-phase PMSM designs with phase numbers equal to five or multiples of three because this allows the associated drive to be formed from multiple conventional three-phase inverters. However, utilizing an H-bridge for each phase potentially improves the reliability because the current in each phase can be controlled independently [2], [18], [19]. Additionally, if each phase is driven by an H-bridge, then any number of phases can be used instead of restricting the choice to a multiple of three. Thus, this paper explores the performance of an unprecedently wide range of slot/pole combinations during both normal operation and operation with an open circuit fault affecting one phase.

An outer rotor topology was selected for evaluation so that the PMSM can be integrated into the bore of a magnetic gear to form a highly reliable powertrain. Using tooth-wound windings eliminates overlapping end turns, which significantly reduces the probability of a phase-to-phase fault. The windings can be double-layer, with a coil wrapped around each tooth, as in Fig. 1(a), or single-layer, with a coil around only every other tooth, as in Fig. 1(b). By introducing a bare tooth, a tooth between each set of windings, the single-layer winding further reduces the likelihood of phase-to-phase faults [16]. Furthermore, Halbach permanent magnet (PM) arrangements, such as the array in Fig. 1, have previously been shown to improve torque density [20] and efficiency [21], and reduce torque ripple [22]. While previous studies compared double-layer and single-layer designs for a single or a few slot/pole combinations [23]-[25], this paper employs an extensive parametric finite element analysis (FEA) study to characterize and compare the performance of the optimal double-layer and single-layer designs in terms of their torque density, power factor (PF), efficiency, and performance in the case of a fault. Additionally, different pole counts, phase numbers, and geometries were evaluated with both conventional (north-south) and Halbach PM arrangements.

Several methods have been developed to control PMSMs during an open phase fault and compensate by adjusting the phases and amplitudes of the currents in the healthy phases to achieve different performance objectives [26]-[30]. Maintaining a constant magnetomotive force (MMF) during the fault is one such control approach, but it results in a higher torque ripple, as discussed in [26], [28], and [30], as well as significantly increased copper losses. Although [26] considered a means of minimizing these losses, the proposed solution also decreased the torque. Past studies [26] and [27] focused on nine- and six-phase motors, where the windings were divided into groups of three. In the case of an open circuit fault in a phase, the control algorithm only changed the currents in the two healthy phases in the three-phase set with

This work was sponsored by the U.S. Army CCDC Army Research Laboratory and was accomplished under Cooperative Agreement Number W911NF-18-2-0289. The views and conclusions contained in this document are those of the authors and should not be interpreted as representing the official policies, either expressed or implied, of the Army Research Laboratory or the U.S. Government. The U.S. Government is authorized to reproduce and distribute reprints for Government purposes notwithstanding any copyright notation herein.

S. Hasanpour, S. Sheshaprasad, B. Praslicka, and H. A. Toliyat are with the EMPE Lab at Texas A&M University, College Station, TX 77843 USA (e-mail: shimahasanpour@tamu.edu, shrikesh@tamu.edu, bryton.praslicka@tamu.edu, toliyat@tamu.edu).

M. C. Gardner was with the EMPE Lab at Texas A&M University, College Station, TX 77843 USA. He is now with the University of Texas at Dallas, Richardson, TX 75080 USA (e-mail: matthew.gardner@utdallas.edu).

M. Johnson is with the U.S. Army CCDC Army Research Lab, College Station, TX 77843 USA (e-mail: matthew.c.johnson186.civ@mail.mil).

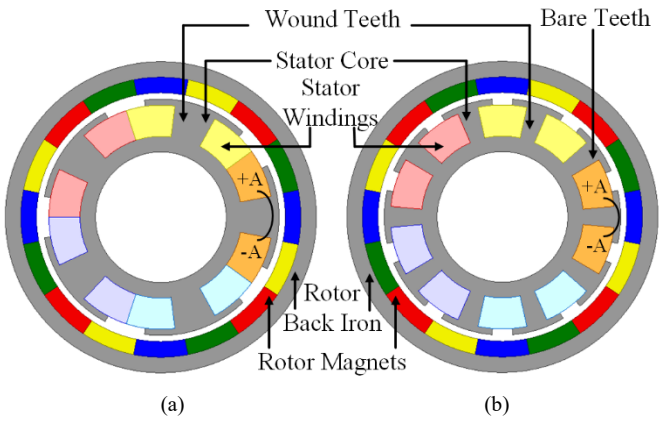

Fig. 1. Cross-sections of an outer rotor PMSM with (a) a double layer winding and (b) a single layer winding.

the fault. This results in a simpler control algorithm, but it also results in increased copper losses and larger torque ripple. This approach also restricts the number of phases to a multiple of three. The control method described in [29] restricts the different phase currents to similar amplitudes and yields lower copper losses, but higher torque ripples.

In this paper, a novel open phase fault current compensation scheme is proposed, in which the phase currents need not sum to zero; the ability to eliminate this constraint is one advantage of utilizing H-bridges. In the proposed scheme, the average torque and torque ripple are kept approximately constant, while the increase in DC copper losses (copper losses neglecting skin effects and eddy currents) is smaller than those experienced in [26]-[30]. Equations are provided to show that this compensation method minimizes the DC copper losses while delivering the rated power.

II. Design Study Methodology

The two topologies shown in Fig. 1 were compared using a parametric design study and 2D finite element analysis (FEA) simulations. For each design, the stack length was scaled to achieve an average torque of 7 N·m. Table I lists the design parameter values used in the parametric sweep, and Table II shows the pole and phase count combinations that were evaluated. However, cases where the number of phases equaled the number of poles or the number of pole pairs (P) would yield excessively large torque ripples; thus, these cases were not considered. The phase count ranges for each number of pole pairs were informed by initial observations and selected to include the optimal phase count within the range. For the double-layer cases, the number of slots is equal to the number of phases, whereas, for the single-layer cases, the number of slots is twice the number of phases.

The primary metrics for evaluating the designs during healthy operation are volumetric torque density (VTD), which is the rotor torque divided by the motor's active volume, specific torque (ST), which is the rotor torque divided by the motor's active mass, efficiency, torque ripple, and PF. All the cases from Tables I and II were initially evaluated using magnetostatic FEA, and the 16,000 best designs based on VTD and ST were evaluated using transient FEA to characterize core losses and power factor. These cases were also evaluated using magnetostatic FEA with a single open phase fault to characterize the effects of this fault on the average torque and torque ripple of the designs.

All designs were simulated using NdFeB N48SH PMs, 29-gauge M19 silicon steel for the ferromagnetic components (rotor back iron and stator core), and copper for the windings. To facilitate air cooling, the rms current density was set to 3.5 A/mm^2 during healthy operation. The current was aligned with the q-axis for maximum torque per ampere (MTPA) operation. In the simulation models, each phase was assumed to have a single series turn. The number and cross-sectional area of the series-connected turns can be adjusted to meet the voltage or current limitations of the drive. As long as the copper fill factor remains constant, this will not affect the efficiency (neglecting AC losses in the windings, which were assumed negligible in this study), power factor or torque of the designs.

The slot opening factor ($\alpha_{Slot\_Opening}$) is defined as the ratio of the slot opening arc length (between adjacent tooth tips) to the arc length of the outer edge of the full slot. For instance, a 0.4 $\alpha_{Slot\_Opening}$ means that 40% of the top arc length of the slot is open and not covered by tooth tips. Also, the tooth fill factor (α_{Tooth}) is the ratio of the angular width of a tooth to the combined angular width of a tooth and a slot. A low α_{Tooth} corresponds to a large area available for the windings, which enables more current for the same current density. Because

TABLE I
Design Parameter Sweep Ranges

Parameter	Description	Range	Units
P	Pole pairs	2-15	
R_{Out}	Active outer radius	50, 70, 90	mm
T_{BI_S}	Stator back iron thickness	5, 10	mm
$T_{Winding}$	Stator winding thickness	10, 15	mm
$T_{ToothTip}$	Tooth tip thickness	1	mm
T_{AG}	Air gap thickness	1	mm
T_{PM}	Rotor magnet thickness	3, 6, 9	mm
T_{BI_R}	Rotor back iron thickness	0, 5, 10	mm
$\alpha_{Slot\_Opening}$	Slot opening factor	0.1, 0.3, 0.5	
α_{Tooth}	Tooth fill factor	0.3, 0.4, 0.5	
α_{Copper}	Copper fill factor	0.5	

TABLE II
Stator Phase Number Sweep Ranges

Pole Pairs	*Number of Phases (N)*	
(P)	*Double Layer*	*Single Layer*
2	3, 5, 6	3, 5
3	4, 5, 7, 8	3, 4, 5
4	3-10	3, 5, 6
5	3-12	3, 4, 6, 7
6	8-14	3-10
7	8-16	3-10
8	10-18	5-10
9	10-20	6-11
10	12-22	6-11
11	12-20	7-12
12	13-23	8-13
13	14-24	9-12
14	19-25	10-15
15	19-26	10-14

higher currents tend to increase the torque density, most of the designs favored lower α_{Tooth} values. The copper fill factor (α_{Copper}) is the fraction of the slot area that is filled with copper.

III. Results

The 2-D FEA magnetostatic simulations determined the initial sizing of the motor for both variations of the topology shown in Fig. 1 (with both north-south PMs and a Halbach array). The legend in Fig. 2 summarizes these different scenarios. The designs on the Pareto front maximizing VTD and maximizing ST at each radius and pole/phase combination were simulated using transient FEA to evaluate efficiency and power factor and under the single open phase fault condition.

A. Normal Operation

Figs. 3(a) and (b) show the maximum VTD and ST achieved in each PM arrangement scenario. The double-layer designs can achieve a slightly higher VTD and ST than the single-layer designs. In a double-layer topology, the number of teeth is the same as the number of phases. However, in a single-layer topology, there are twice as many teeth as there are phases. Therefore, the windings do not cover the bare teeth in the single-layer topology and the equivalent current flowing around those teeth, which is the resultant of the currents flowing in the two adjacent windings, is less than the current flowing around the other teeth. This difference results in slightly different maximum VTDs and STs for the double-layer and single-layer topologies. Employing the Halbach array on the rotor improves the torque density of both topologies, especially at higher rotor pole pair counts, as shown in Figs. 3(a) and (b). The Halbach array increases the air gap flux and reduces the flux in the rotor back iron. As the rotor pole pair counts increase, the arc lengths of the PMs decrease. Thus, the tangential portions of the flux paths get shorter, and the Halbach arrays can provide an adequate return path for the flux, eliminating the need for the rotor back iron. Figs. 3(a) and 3(b) also indicate that the maximum achievable VTD and ST exhibit similar trends with respect to pole pair count and Halbach arrays.

The following figures show the values of various parameters corresponding to each of the optimal VTD designs. Fig. 4(a) displays the corresponding number of phases for the optimal designs in Fig. 3(a). The single-layer designs have much lower optimal phase counts than the double-layer designs. However, comparing the cross-sectional areas of the windings shows that the winding area of the single layer topology is same as the winding area of the double layer topology with twice the number of phases. The teeth separating windings in the single-layer designs may increase the reliability by preventing adjacent phases from being affected if there is a short circuit in a winding. However, the higher number of phases in the optimal double-layer designs provides more redundancy in the case of open circuit faults.

The maximum VTD designs have the maximum simulated outer radius, except in the case of the optimal double-layer designs with 2 pole pairs, so the stack lengths are generally inversely proportional to the VTD, as shown in Fig. 4(b).

Figs. 5(a) and 5(b) show how the phase count affects the maximum achievable VTD for the double-layer and single-layer topologies with Halbach arrays. For better visualization, only 4 rotor pole pair counts are illustrated. For some pole pair counts, the VTD is maximized with a number of phases that is not a multiple of 3. Thus, considering a wide range of phases can yield higher VTDs, at the expense of requiring an unconventional inverter.

	Double-Layer Winding	Single-Layer Winding
Conventional PMs		
Halbach Array PMs		

Fig. 2: Legend for the design trend plots in Figs. 3-8.

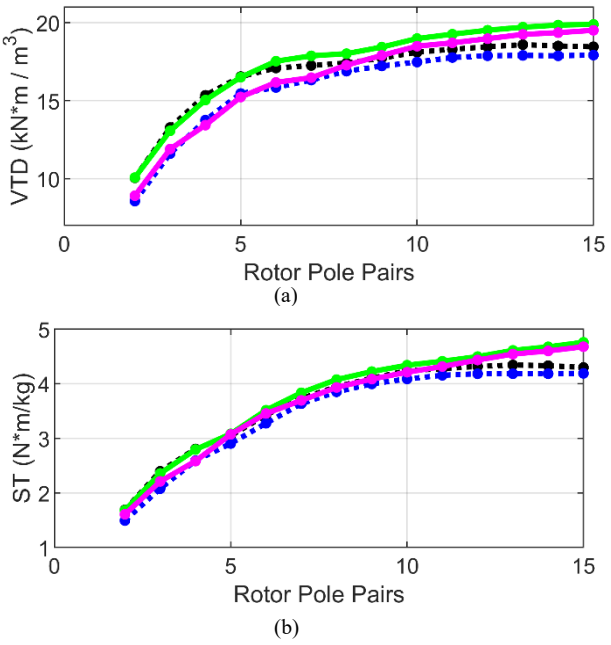

Fig. 3. Impact of rotor pole pair count on the maximum acheiveable (a) VTD and (b) ST of the topologies with conventional or Halbach array PMs.

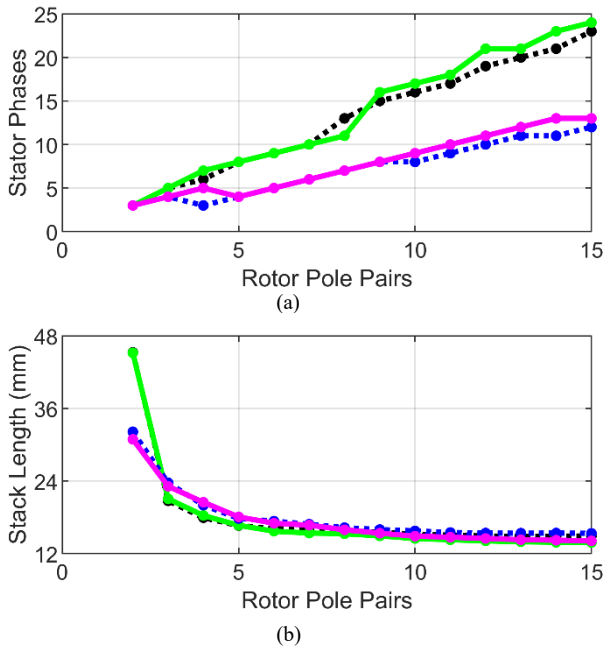

Fig. 4. Corresponding (a) stator phase numbers and (b) stack lengths for the maximum VTD designs shown in Fig. 3(a).

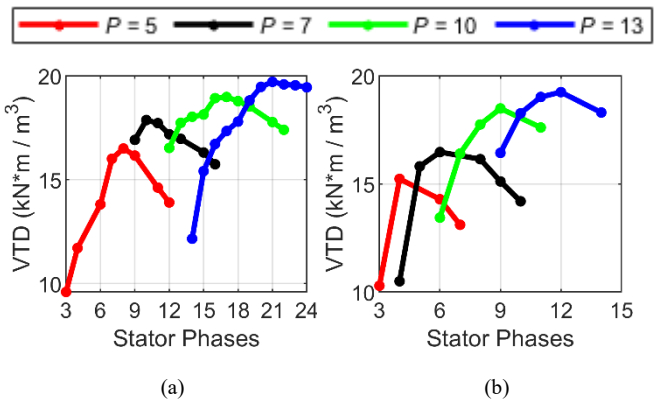

Fig. 5. Impact of stator phases on the maximum achieveable VTD for (a) double-layer designs and (b) single-layer designs with Halbach arrays.

Fig. 6 shows the PF for both topologies and PM arrangements during MTPA operation. Due to the surface mounted PMs, the inductances are relatively low, so the PFs are relatively high, especially for designs with thicker PMs. The Halbach array designs with maximum PF use thicker PMs than the conventional PM designs with maximum PF.

Fig. 7(a) depicts the electromagnetic efficiencies (not including friction or windage) of the optimal VTD designs at full load (7 N·m) and rated speed (1800 rpm). Figs. 7(b)-7(d) show the per unit (pu) copper loss, PM loss, and core loss of the same designs in Fig. 7(a), where the pu loss is defined as the ratio of the losses to the output power (1.3 kW for all designs). The DC copper losses decrease as the pole pairs increase, due to the increased VTD, which reduces the copper volume. Additionally, the number of slots in the optimal designs increases with the number of pole pairs, which reduces the length of the end windings. The eddy current losses in the PMs are unexpectedly high, which reduces the efficiency significantly, especially in the designs with lower pole pair

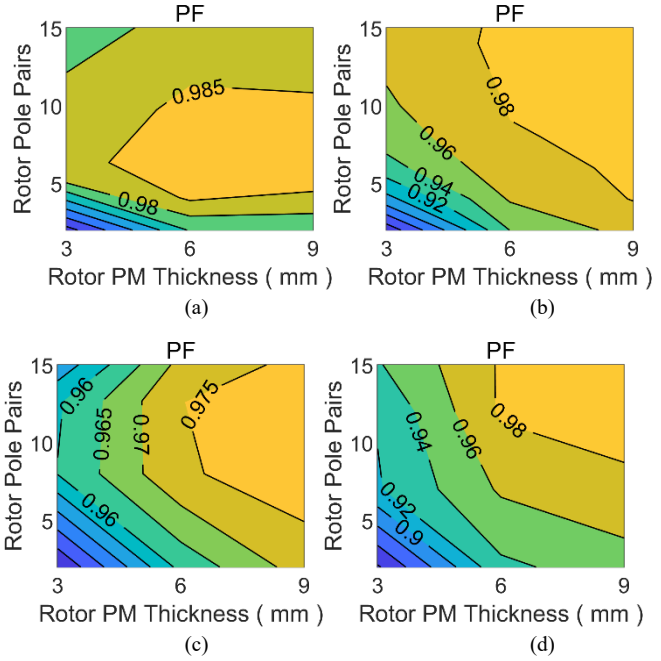

Fig. 6. Variation of PF for the maximum VTD designs using (a) a double-layer winding with conventional PMs, (b) a double-layer winding with a Halbach array, (c) a single-layer winding with conventional PMs, and (d) a single-layer windings with a Halbach array.

counts. This likely occurs because the 2D simulation does not account for the finite axial length of the PMs when computing the eddy current losses in the PMs. Furthermore, the PM losses could be reduced by segmenting the magnets or optimizing the shape of tooth tips. This is illustrated by the fact that the Halbach array designs, which have twice as many PM pieces as the conventional PM designs, have significantly lower PM eddy current losses than the conventional north-south designs. Additionally, the PM eddy current losses tend to decrease as pole pair count increases, reducing the arc length of each PM. The core losses in the rotor back iron and stator increase with the pole pair count, due to the increase in electromagnetic frequency. However, the core losses tend to be significantly smaller than the other losses, except at the very highest pole counts. Overall, the designs with Halbach arrays and high pole counts are able to achieve good efficiencies, and the other

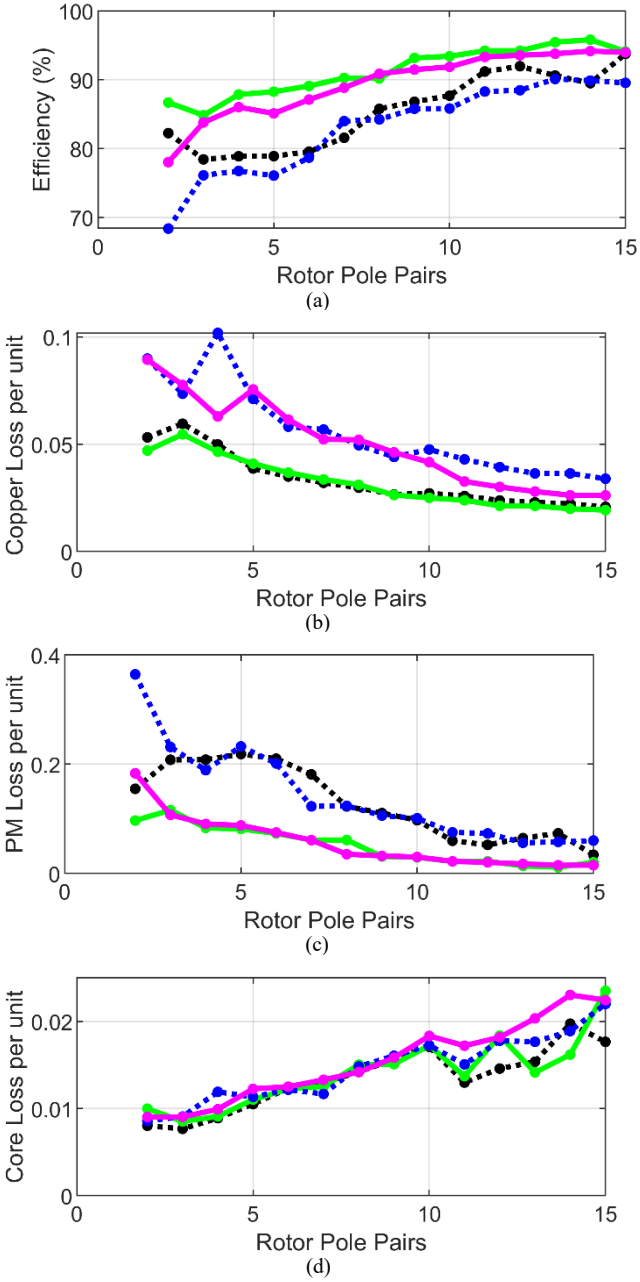

Fig. 7. Corresponding (a) efficiency, (b) DC copper losses, (c) PM losses, and (d) core losses for the maximum VTD designs shown in Fig. 3(a).

designs could likely achieve acceptable efficiencies if the PM eddy current losses were reduced by segmenting the PMs.

B. Short Circuit Fault

One important tradeoff to consider when designing a PMSM is that using thicker magnets results in lower inductance and higher PF, but the smaller inductance also leads to a higher short circuit current. A short circuit fault in can cause a cascading failure by further damaging the insulation or demagnetizing the PMs. Fig. 8 shows the characteristic current in one phase, where the per unit ratio is defined as the ratio of the RMS characteristic current to the nominal RMS current. The designs with Halbach arrays favor thicker magnets and, for the higher pole counts, air cores (no rotor back irons). Thus, the Halbach array designs tend to have lower inductances and higher characteristic currents. The single-layer designs also tend to have smaller per unit characteristic currents than the double-layer designs because the windings in the optimal single-layer designs have larger cross sections, which results in higher nominal currents. Thus, the single-layer designs' per unit characteristic currents are lower than those of the double-layer designs, even though their back emfs and inductances are in the same ranges. The characteristic currents in Fig. 8 are too high; this should be considered in future optimization studies.

C. Open Circuit Fault

An open circuit fault in one of the switches or windings can result in the machine operating with one less phase than normal. Alternatively, a machine may stop using one of its phases if an incipient fault in that phase is detected. In either case, the loss of one phase will reduce the torque produced by the machine and increase the torque ripple. However, these issues can be mitigated by appropriately increasing the current in the remaining healthy phases, but this results in increased DC copper losses and, potentially, local saturation.

There are several approaches to calculate the compensating current in the other phases when one phase has no current [26]-[30]. The goal is to maintain the same average torque without significantly increasing the torque ripple or DC copper losses. In one of the evaluated motors with N phases and P pole pairs, the per unit healthy current phasor in phase n can be determined based on the electromagnetic angle of the tooth the phase is wound around, as in (1).

$$\bar{I}_{n,h} = e^{-j(n-1)\cdot\frac{2\pi}{N}\cdot P} \tag{1}$$

When phase 1 is open, the currents in the other phases can be adjusted to compensate and maintain the same average torque with a similar torque ripple. Each remaining healthy phase ($n \geq 2$) is adjusted in the direction of the phase 1 current phasor by an amount proportional to the cosine of the angle between the healthy current phasor for that phase and the phase 1 current phasor. Thus, (2) gives the adjusted per unit current phasors for the remaining healthy phases.

$$\bar{I}_{n,f} = e^{-j(n-1)\cdot\frac{2\pi}{N}\cdot P} + \frac{\cos(n-1)\cdot\frac{2\pi}{N}\cdot P}{\sum_{n=2}^{N}\left(\cos(n-1)\cdot\frac{2\pi}{N}\cdot P\right)^2} \tag{2}$$

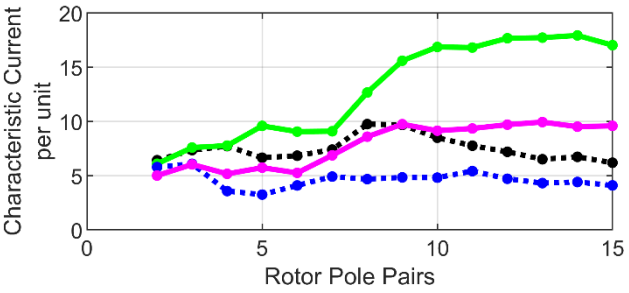

Fig. 8. Corresponding characteristic currents for the maximum VTD designs shown in Fig. 3(a).

Increasing the number of phases generally reduces the current compensation required for each phase. Because the DC copper losses increase with the current squared, their increase is largest for the designs with the fewest phases, as depicted in Fig. 9. Also, the large current compensations in the designs with fewer phases are more likely to produce saturation and increase torque ripple than the smaller current compensations in the designs with more phases. One design for each topology from Fig. 3(a) is characterized in Table III. Phasor diagrams of the current in each winding before and after the open circuit fault are provided for each design in Table III. Additionally, the torque waveforms for a full electromagnetic period are presented for both healthy and faulted operation. The ability to maintain the average torque without a significant increase in torque ripple demonstrates the proposed current compensation's effectiveness. The increase in DC copper losses is smaller than those incurred using the approaches in similar studies [26]-[30].

A case with 4 pole pairs and 5 phases is presented to illustrate the optimality of (2). The current phasors for healthy operation are shown in Fig. 10(a). When the current in phase 1 goes to zero, the currents in the other phases are increased to compensate for the power that phase 1 supplied. To keep the ripple from drastically increasing, the instantaneous power, not just the average power, is kept constant. Thus, the currents in the remaining healthy phases are increased in the direction parallel to the phase 1 current phasor. Due to symmetry, the increase in phase 2 mirrors the increase in phase 5, and the increase in phase 3 mirrors the increase in phase 4. This results in two degrees of freedom for the current increases, shown as x and y in Fig. 10(b). For MTPA operation, the healthy current phasor aligns with the back emf for each phase. Thus, the pu power contributions of the current compensations in phases 2-5 can be expressed as the left-hand side of (3) when phase 1 would normally have its maximum current; to keep the same instantaneous power, the right-hand side is set to unity. The

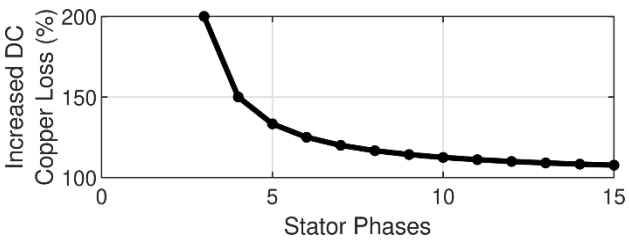

Fig. 9. Percentage increase in DC copper losses during faulted operation for the maximum VTD designs in Fig. 3(a).

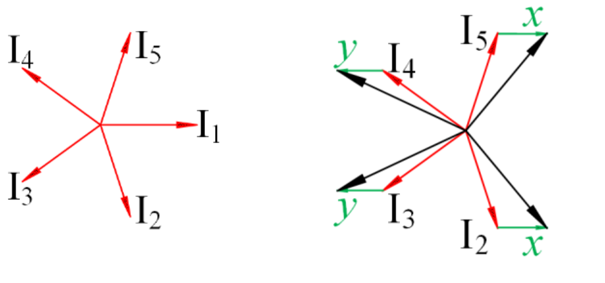

(a) (b)

Fig. 10. Current vectors of a 4 pole pair, 5 phases PMSM during (a) healthy operation and (b) a phase 1 open circuit.

per unit average DC copper losses, P_{Cu}, for the currents in Fig. 10(b) are given in (4), where R is the per unit phase resistance. Solving for y in (3), substituting it into (4), and setting the derivative of (4) with respect to x equal to 0 yields (5), which agrees with (2) for the 5-phase case. Thus, for this example, (2) maintains the same instantaneous power with the minimum increase in copper losses.

$$2x\cos(72°) + 2y\cos(144°) = 1 \quad (3)$$

$$P_{cu} = 2R(\sin(72°)^2 + (x + \cos(72°))^2) + 2R(\sin(144°)^2 + (y + \cos(144°))^2) \quad (4)$$

$$x = \frac{\cos(72°)}{2\cos^2(72°) + 2\cos^2(144°)} \quad (5)$$

IV. Conclusion

This paper analyzes the performance of multi-phase PMSMs with double-layer and single-layer windings. The topologies are optimized with independent selection of pole pair and phase counts. An H-bridge is used to drive each phase, allowing more flexible control in the case of a fault. The H-bridges and large number of phases require a large number of switches. Thus, this approach may be best suited for high power motors, where it is necessary to use a large number of switches with reduced power ratings. The FEA results yield the following conclusions:

- Double-layer windings can yield higher torque densities and efficiencies than single-layer windings. Allowing the phase numbers to vary freely (not just multiples of 3) can increase the torque density.
- Using Halbach arrays improves the torque density and efficiency, but increases the characteristic circuit current.
- Equation (2) proposes a closed-form novel open circuit fault compensation scheme for any slot/pole combination that maintains the same average torque and torque ripple with a minimal increase in DC copper losses.

Future work includes system-level analysis of the benefits and disadvantages of using an H-bridge for each phase.

V. Acknowledgement

Portion of this research were conducted with the advanced computing resources provided by Texas A&M High Performance Research Computing. The authors would like to thank ANSYS for their support of the EMPE lab through the provision of FEA software.

TABLE III
COMPARISON OF PERFORMANCES DURING NORMAL OPERATION AND WITH AN OPEN CIRCUIT FAULT

	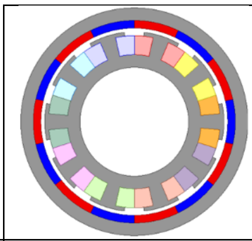	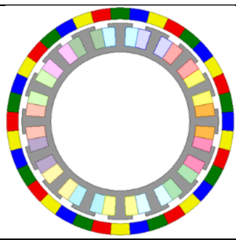	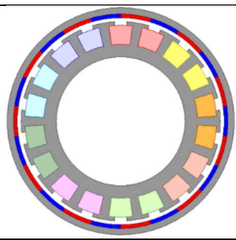	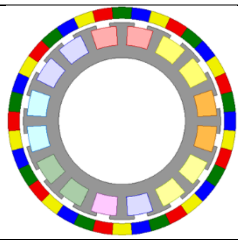
P = Pole Pairs N = Phases	P = 7 N = 10	P = 9 N = 16	P = 11 N = 9	P = 9 N = 8
Current Phasor Diagram During Normal Operation (red) and Operation with an Open Circuit Fault (black)	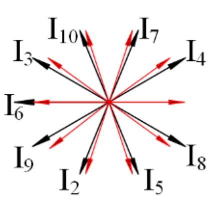	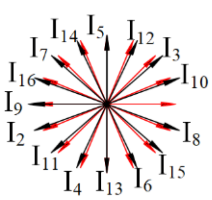	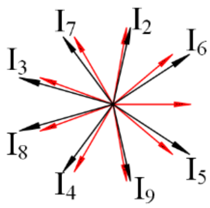	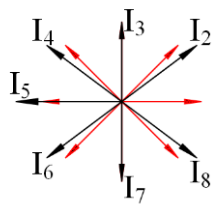
Torque vs Rotational Angle Normal Operation Open Circuit Fault	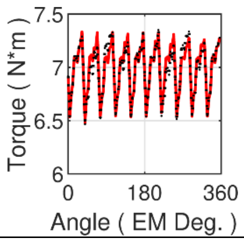	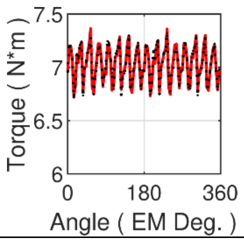	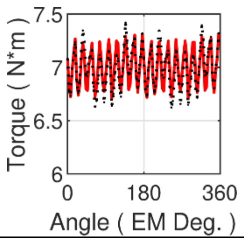	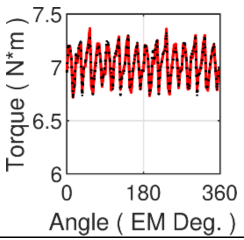
DC Copper Loss Increase	12%	7%	14%	16%

VI. REFERENCES

[1] B. C. Mecrow, A. G. Jack, J. A. Haylock and J. Coles, "Fault tolerant permanent magnet machine drives," in *Proc. IEEE Int. Elect. Mach. Drives Conf.*, 1995, pp. 433-437.

[2] X. Jiang, D. Xu, L. Gu, Q. Li, B. Xu and Y. Li, "Short-circuit fault-tolerant operation of dual-winding permanent-magnet motor under the four-quadrant condition," *IEEE Trans. Ind. Electron.*, vol. 66, no. 9, pp. 6789-6798, Sept. 2019.

[3] J. Xu, B. Zhang, H. Fang and H. Guo, "Guaranteeing the fault transient performance of aerospace multiphase permanent magnet motor system: An adaptive robust speed control approach," in *CES Trans. Elect. Mach. Syst.,* vol. 4, no. 2, pp. 114-122, June 2020.

[4] A. Mohammadpour, A. Gandhi and L. Parsa, "Design and control of fault-tolerant permanent magnet machines," *IEEE Workshop Elect. Mach. Des., Control and Diagnosis*, 2013, pp. 108-116.

[5] L. Jin, S. Norrga, H. Zhang and O. Wallmark, "Evaluation of a multiphase drive system in EV and HEV applications," in *Proc. IEEE Int. Elect. Mach. Drives Conf.*, 2015, pp. 941-945.

[6] B. Anvari, Y. Li and H. A. Toliyat, "Design of multiphase exterior rotor switched reluctance motor for traction applications," in *Proc. Int. Symp. Ind. Electron.*, 2016, pp. 161-166.

[7] L. Parsa and H. A. Toliyat, "Five-phase interior permanent magnet motor with low torque pulsation," *IEEE Ind. Appl. Conf.*, 2005.

[8] I. Bolvashenkov, J. Kammermann, S. Willerich and H-G. Herzog,"Comparative study of reliability and fault tolerance of multiphase permanent magnet synchronous motors for safety-critical drive trains", in *Proc. Int. Conf. Renewable Energies and Power Quality*, 2016, pp. 1–6.

[9] G. Q. Bao and J. Z. Jiang, "A modular multiphase permanent magnet machine optimization for direct propulsion systems," in *Proc. IEEE Veh. Power and Propulsion Conf.*, 2008, pp. 1-5.

[10] Q. Chen, G. Liu, W. Gong and W. Zhao, "A new fault-tolerant permanent-magnet machine for electric vehicle applications," *IEEE Trans. Magn.*, vol. 47, no. 10, pp. 4183-4186, Oct. 2011.

[11] J. Kammermann, I. Bolvashenkov, J. L. Ugalde and H. -G. Herzog, "Choice of phase number for a multiphase traction motor to meet requirements on fault tolerance," in *Proc. Int. Conf. Electrotechnical Complexes and Syst*., 2019, pp. 1-6,

[12] Y. Demir and M. Aydin, "Design, analysis and validation of a dual three-phase 72-slot, 12-pole permanent magnet synchronous motor," in *Proc. Int. Conf. Elect. Mach*., 2016, pp. 1598-1603.

[13] E. Yolacan, Y. Demir and M. Aydin, "Design, FEA and dynamic simulation of a new unconventional 9-phase PMSM with asymmetric winding," in *Proc. Int. Conf. Elect. Mach*., 2018, pp. 2123-2129.

[14] M. T. Bin Tarek and S. Choi, "Design and rotor shape modification of a multiphase high speed permanent magnet assisted synchronous reluctance motor for stress reduction," in *Proc. IEEE Energy Convers. Congr. Expo*., 2017, pp. 5389-5395.

[15] L. Zhang, Y. Fan, R. D. Lorenz, A. Nied and M. Cheng, "Design and comparison of three-phase and five-phase FTFSCW-IPM motor open-end winding drive systems for electric vehicles applications," *IEEE Trans. Veh. Technol*., vol. 67, no. 1, pp. 385-396, Jan. 2018.

[16] M. Villani, M. Tursini, G. Fabri and L. Castellini, "High reliability permanent magnet brushless motor drive for aircraft application," *IEEE Trans. Ind. Electron*., vol. 59, no. 5, pp. 2073-2081, May 2012.

[17] S. S. R. Bonthu, S. Choi and J. Baek, "Design optimization with multiphysics analysis on external rotor permanent magnet-assisted synchronous reluctance motors," *IEEE Trans. Energy Conv.*, vol. 33, no. 1, pp. 290-298, March 2018.

[18] S. Koschik, F. Adler, D. Szepanski, and R. W. De Doncker, "Scalable FPGA and DSP based control for multiphase concentrated winding permanent magnet machines with single coil integrated inverters," in *Proc. IEEE Int. Elect. Mach. Drives Conf.*, 2015, pp. 1515-1521.

[19] M. D. Hennen, M. Niessen, C. Heyers, H. J. Brauer, and R. W. De Doncker, "Development and control of an integrated and distributed inverter for a fault tolerant five-phase switched reluctance traction drive," *IEEE Trans. Power Electron.*, vol. 27, no. 2, pp. 547-554, Feb. 2012.

[20] K. Liu, M. Yin, W. Hua, Z. Ma, M. Lin and Y. Kong, "Design and analysis of Halbach ironless flywheel BLDC motor/generators," *IEEE Trans. Magn*., vol. 54, no. 11, pp. 1-5, Nov. 2018.

[21] A. Hebala, S. Nuzzo, P. H. Connor, P. Giangrande, C. Gerada and M. Galea, "PM Halbach arrays in motors:loss reduction and performance improvements," in *Proc. Int. Conf. Elect. Mach. Syst*., 2020, pp. 710-715.

[22] H. T. Wang, S. H. Fang, B. C. Guo and H. Y. Lin, "A new Halbach arc permanent magnet synchronous motor with three-dimensions air gap used on large telescope," in *Proc. Int. Conf. Appl. Supercond. Electromagn. Devices*, 2015, pp. 478-479.

[23] H. Chen, X. Liu, A. M. EL-Refaie, J. Zhao, N. A. O. Demerdash, and J. He, "Comparative study of winding configurations of a five-phase flux-switching PM machine," *IEEE Trans. Energy Conv.*, vol. 34, no. 4, pp. 1792-1804, Dec. 2019.

[24] A. G. Sarigiannidis, M. E. Beniakar, P. E. Kakosimos, A. G. Kladas, L. Papini, and C. Gerada, "Fault tolerant design of fractional slot winding permanent magnet aerospace actuator," *IEEE Trans. Transp. Electri.*, vol. 2, no. 3, pp. 380-390, Sept. 2016.

[25] J. Yang et al., "Quantitative comparison for fractional-slot concentrated-winding configurations of permanent-magnet Vernier machines," *IEEE Trans. Magn.*, vol. 49, no. 7, pp. 3826-3829, July 2013.

[26] F. Li, W. Hua, M. Cheng and G. Zhang, "Analysis of fault tolerant control for a nine-phase flux-switching permanent magnet machine," *IEEE Trans. Magn.*, vol. 50, no. 11, pp. 1-4, Nov. 2014.

[27] C. Tong, F. Wu, P. Zheng, Y. Sui and L. Cheng, "Analysis and design of a fault-tolerant six-phase permanent-magnet synchronous machine for electric vehicles," in *Proc. Int. Conf. Elect. Mach. Syst*., 2014, pp. 1629-1632.

[28] J. Fu and T. A. Lipo, "Disturbance free operation of a multiphase current regulated motor drive with an opened phase," in *Proc. IEEE Ind. Appl*, 1993, pp. 637-644 vol.1,

[29] A. Akay and P. Lefley, "Research on torque ripple under healthy and open-circuit fault-tolerant conditions in a PM multiphase machine," in *CES Trans. Elect. Mach. Syst.*, vol. 4, no. 4, pp. 349-359, Dec. 2020.

[30] A. Akay, P. Lefley and M. Kansara, "Open-circuit fault-tolerant control for a five-phase permanent magnet synchronous machine drive," in *Proc. Int. Conf. Elect. Electron. Eng*., 2020, pp. 150-154.

VII. BIOGRAPHIES

Shima Hasanpour (S' 18) earned her B.S. in electrical engineering from Sharif University of Technology, Tehran, Iran in 2018. She is currently pursuing a Ph.D. in electrical engineering while working in the Advanced Electric Machines and Power Electronics Laboratory at Texas A&M University. Her research interests include the optimal design and control of electric machines, magnetic gears, and magnetically geared machines.

Shrikesh Sheshaprasad (S' 21) earned his B.S. in electrical engineering from RV College of Engineering, Bangalore, India in 2019. He is currently pursuing a Ph.D. in electrical engineering while working in the Advanced Electric Machines and Power Electronics Laboratory at Texas A&M University. His research interests include design and control of electric machines, magnetic gears and power electronics.

Matthew C. Gardner (S' 15, M' 19) earned his B.S. in electrical engineering from Baylor University, Waco, Texas in 2014. He earned his Ph.D. in electrical engineering from Texas A&M University, College Station, Texas in 2019. His research interests include optimal design and control of electric machines and magnetic gears.

Matthew Johnson (S' 13, M'17) earned his B.S. and Ph.D. both in electrical engineering from Texas A&M University, College Station, Texas, in 2011 and 2017, respectively. He is currently an electronics engineer for the U.S. Army Research Laboratory. His research interests include the design and control of electric machines and magnetic gears.

Bryton Praslicka (S' 20) earned his B.S. in electrical engineering from Texas A&M University, College Station, Texas in 2019. He is currently pursuing a Ph.D. in electrical engineering while working in the Advanced Electric Machines and Power Electronics Laboratory at Texas A&M University. His research interests include the optimal design and control of electric machines, magnetic gears, and magnetically geared machines.

Hamid A. Toliyat (S'87, M'91, SM'96, F'08) received the B.S, degree from Sharif University of Technology, Tehran, Iran in 1982, the M.S. degree from West Virginia University, Morgantown, WV in 1986, and the Ph.D. degree from University of Wisconsin-Madison, Madison, WI in 1991, all in electrical engineering. In March 1994 he joined the Department of Electrical and Computer Engineering, Texas A&M University where he is currently the Raytheon endowed professor of electrical engineering. Dr. Toliyat has many papers and awards to his name, including the Nikola Tesla Field Award.